Synthesis and Properties of $BaFe_{12}O_{19}$ Thick Films for Microwave Electronics and Terahertz Spectroscopy

Vladimir G. Kostishin*, Vitalii A. Turchenko, Elena S. Savchenko, Igor M. Isaev, Andrei Yu. Mironovich, Alexander G. Savchenko, Alexei D. Prusakov, Maxim A. Sysoev, Alexei A. Smirnov and Savva D. Morozov

National Research and Technology University MISiS, 4 Leninskiy Prospekt, 119049 Moscow, Russia

Abstract: Isotropic polycrystalline $BaFe_{12}O_{19}$ films with thicknesses of 19, 20, 39, 41 and 485 μm were obtained by slip casting on Al_2O_3 substrates in three process modes. The crystal structure, surface quality and magnetic hysteresis loop parameters of the specimens were studied using X-ray diffraction, optical microscopy and vibromagnetometry. The quality and properties of the as-synthesized specimens and those grown in different process modes were studied. Films grown in Mode 2 proved to have the highest magnetic parameters and surface quality. The specific saturation magnetization of these films was σ_s = 73÷76 emu/g, the magnetization coercive force was $_iH_c$ = 3.07÷3.08 kOe and the magnetic texture degree was *f* = 11.82÷15.76%.

Keywords: Barium hexaferrite thick films, Slip casting, Magnetic hysteresis loops, X-ray phase analysis, Lattice parameter, Coercive force, Remanence magnetization, Magnetic texture degree.

1. INTRODUCTION

The crystal structure of M-type hexagonal barium ferrite $BaFe_{12}O_{19}$ (BaM) is isomorphic to that of magnetoplumbite $PbFe_{12}O_{19}$ [1, 2]. Due to its unique magnetic and electromagnetic properties, BaM finds wide application in permanent magnets, active media of microwave electronics and terahertz photonics [2-9]. The operation of BaM-containing microwave electronics devices (valves, resonators, attenuators etc.) is based on the ferromagnetic resonance effect or the Faraday effect occurring in BaM at operation frequencies of 30-60 GHz [3, 5-8]. The use of hexaferrites as active media of millimeter wavelength range microwave electronics devices allows one to not use external magnetic systems, due to the high inner magnetic fields of hexaferrites, thus substantially reducing the dimensions and cost of the devices [10, 11].

In recent decades, there has been a trend to use BaM thick films instead of BaM hexagonal ferrite bulk poly- and single crystals in microwave electronics devices (including those for the millimeter wavelength range). This replacement is purposeful since the use of BaM thick films instead of bulk materials improves the performance, reduces the cost and increases the compatibility of the devices with planar semiconductor electronics devices [12, 13].

BaM thick films are also promising materials for components and devices of terahertz spectroscopy and magnonics.

High-quality anisotropic BaM thick films can be synthesized using sputtering techniques, the sol-gel method or pulse laser deposition (PLD) [14-16]. These methods allow low-loss deposition of BaM films, but the thickness of the as-synthesized films is within 200 nm. However, achieving the best microwave properties of millimeter wavelength range circulators requires the thickness of the films be 1 μm or greater. Furthermore, films deposited using the above techniques undergo cracking or exfoliation as their thickness increases, leading to their degradation of the magnetic and microwave properties. Vacuum techniques (PLD, sputtering) are quite costly, labor-intensive and deliver low growth rates, whereas the sol-gel method has low efficiency [17]. The above methods are suitable for lab work, not for commercial applications.

The screen printing technique allows growing thick BaM films and is relatively simple in implementation [12, 13, 18]. However, films grown using this method exhibit high microwave losses and are typically not self-biased.

The aim of this work was to grow BaM thick films by slip casting and to study their structure and properties.

2. PREPARATIONS AND CHARACTERIZATION OF SAMPLES

Figure **1** shows the process route of $BaFe_{12}O_{19}$ films. It should be noted that the slip casting method is preferable both in terms of productivity and in terms of controlling the thickness and dimensions (area) of the formed film.

The raw material was barium hexaferrite powder synthesized using a standard ceramics technology [1, 5, 19], with the iron-containing raw material being

*Address correspondence to this author at the National Research and Technology University MISiS, 4 Leninskiy Prospekt, 119049 Moscow, Russia; E-mail: drvgkostishyn@mail.ru

Received on 04-10-2026 Accepted on 13-11-2026 Published on 17-11-2026

E-ISSN: 2410-4701/26

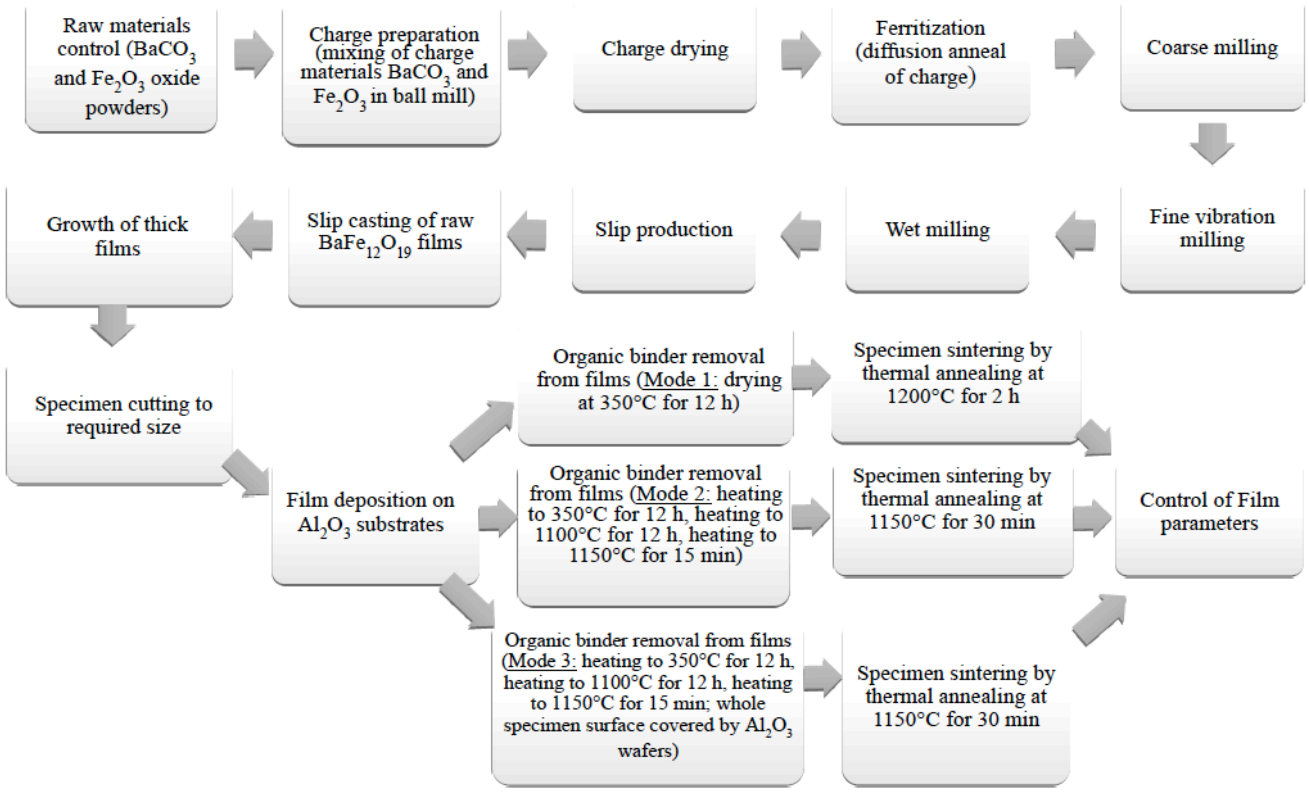


Figure 1: $BaFe_{12}O_{19}$ thick film slip casting process route (three process modes).

MM-2 Grade iron oxide Fe_2O_3 (TU6-09-4816-80, impurity content, wt.%: SiO2 – 0.01; Al2O3 – 0.01; Cr2O3 – 0.01; Na2O – 0.01) and the barium source being barium carbonate $BaCO_3$ (≥ 99.5 % purity, GOST 2149-75).

The optimum combination of magnetic properties in $BaFe_{12}O_{19}$ is observed for high-BaO compositions [19].

Thus, the charge was composed in accordance with the following formula: BaO·(5.5÷5.75)Fe2O3. After thorough ball mill mixing of the raw oxides, the charge was dried and ferritized (Figure **1**) in a muffle furnace in an air atmosphere at 950 °C for 2.5 h. After ferritization, the ferrite powder was coarse, fine and wet milled and dried at 110 °C.

The film-forming agent for slip production was polyvinyl butyral, the solvent being ethyl alcohol, butyl acetate and dibutyl phthalate. The ratio between $BaFe_{12}O_{19}$ and the film-forming agent + solvent mixture was 70/30. The slip was agitated for 8 h.

Slip casting synthesis of barium hexaferrite $BaFe_{12}O_{19}$ films was carried out using a CAM-M1A instrument from KekoEquipment Ltd., Slovenia (Figure **2a**). The films were cast onto a Lavsan ribbon with a silicon layer, followed by drying at 50 °C. The 9-15 μm as-cast film thickness was achieved by choosing the blade height and the Lavsan ribbon speed. The film specimen thickness was further increased by compressing as-cast films with a PAL-9DB instrument from KekoEquipment Ltd., Slovenia (Figure **2b**) followed by hydrostatic compression at 40 MPa.

During compression the working film was separated from the Lavsan ribbon. The resultant raw billets were 30x30 cm in size and 20, 40 and 500 μm in thickness. For further studies, the billets were cut into ~1x1 and ~2x2 cm specimens.

The next two important process steps were organic binder removal and sintering. Three process modes were used in order to find the best process conditions (Figure **1**):

1. Mode 1. Organic binder was removed by holding the specimens in a resistive furnace at 350 °C for 12 h. Then the temperature was raised to 1200 °C, and the specimens were sintered for 2 h.

2. Mode 2. Organic binder was removed by heating the specimens in a resistive furnace from room temperature to 350 °C for 12 h. Then the temperature was raised to 1100 °C for 12 h and then to 1150 °C for 15 min. The specimens were then sintered at 1150 °C for 30 min.

3. Mode 3. Identical to Mode 2, except that the whole specimen surface was covered (pressed down) with Al_2O_3 plates during organic binder removal and sintering.

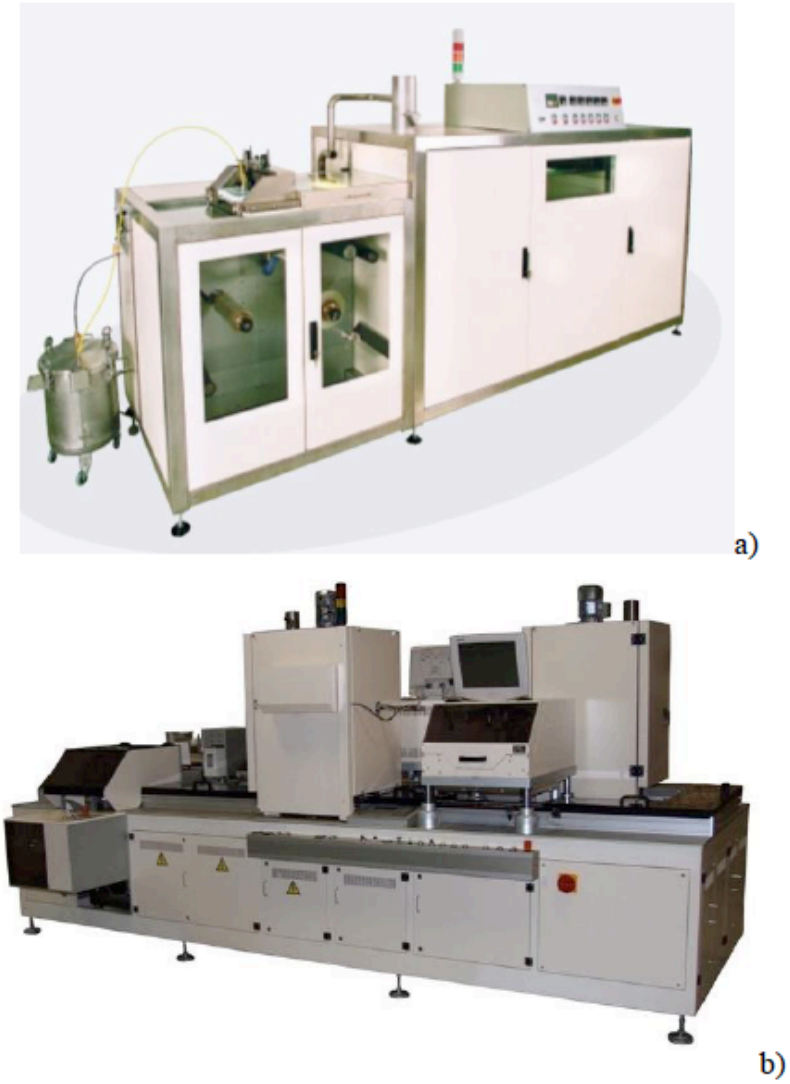


Figure 2: $BaFe_{12}O_{19}$ thick film slip casting instruments; **a**) film casting machine; **b**) stacking machine.

Table 1: Initial Information on BaM Thick Film Specimens

#	Specimen Notation	Thickness h, μm	Process Mode	Sintering Weight Loss (shrinkage), %	NOTES
1.	2-1	20	–	–	Raw film (before binder removal and sintering)
2.	2-2	39	Mode 1	20.70	–
3.	2-3	485	Mode 2	21.38	–
4.	2-4	19	Mode 2	20.33	–
5.	2-5	20.5	Mode 3	17.60	–
6.	2-6	41	Mode 3	18.75	–

After furnace cooling, the specimens were controlled and characterized. All in all, 6 specimens were chosen for studies. Data on the specimens are summarized in Table **1**.

Binder removal and sintering cause shrinkage, *i.e.*, a reduction in the weight and dimensions of the specimens. The shrinkage of the specimens obtained in this work was from 17.6 to 21.38%. It was typical that the specimens treated in Mode 3 exhibited the smallest weight loss.

3. RESULTS AND DISCUSSION

3.1. Crystal Structure of Obtained BaM Films

The crystal structure of the obtained BaM films was studied on an Empyrean X-ray diffractometer from

PANalytical in Cu $\lambda_{\alpha 1}$ (1.540560 Å) and Cu $\lambda_{\alpha 2}$ (1.544390 Å) at room temperature. Data acquisition time was ~3000 sec at each point, with a 0.026 deg step. The experimental data were analyzed with High Score Plus [20] and Full Prof [21] software and compared with ICDD diffraction database [22] in order to identify the phase composition and correct the structure parameters of the test materials, *i.e.*, lattice parameter and microstructure.

The microdeformation of the films was calculated in the Williamson–Hall approximation from the slope angle of the broadening vs diffraction angle curve (Eq. (1)):

$$\beta \cos(\theta) = K\frac{\lambda}{D} + 4\varepsilon \sin(\theta), \quad (1)$$

where β is the true physical diffraction peak broadening of the film. The resolution of the X-ray diffractometer was determined based on the diffraction peak broadening for LaB_6 powder.

Magnetic hysteresis of the specimens was studied at room temperature with a VSM-250 vibrating sample magnetometer from YP Magnetic Technology Development Co., Ltd, China.

The magnetic texture degree *f* of the specimens was calculated from the hysteresis loop parameters using the following formula [23]:

$$f = \left(1 - \frac{B_{r\perp}}{B_{r\parallel}}\right) \cdot 100\%, \quad (2)$$

where $B_{r\perp}$ and $B_{r\parallel}$ are the magnetic induction figures perpendicular and parallel to the specimen plane, respectively.

Figure **3** a shows general X-ray diffraction patterns for the BaM film specimens.

The results suggest that all the test films had a hexagonal crystal structure with the space group $P6_3/mmc$ (No. 197), corresponding to the $BaFe_{12}O_{19}$ phase, (ICDD 98-015-7056). The raw film specimen (2-1) and specimens 2-2 through 2-4 obtained in Modes 1 and 2 are single-phase, whereas the specimens grown in Mode 3 exhibit the Fe_2O_3 impurity (ICDD 98-041-5251), see Figure **3b**. The appearance of the α-Fe_2O_3 impurity phase only in samples prepared under Mode 3 indicates that this mode leads to the partial decomposition of hexaferrite or to the

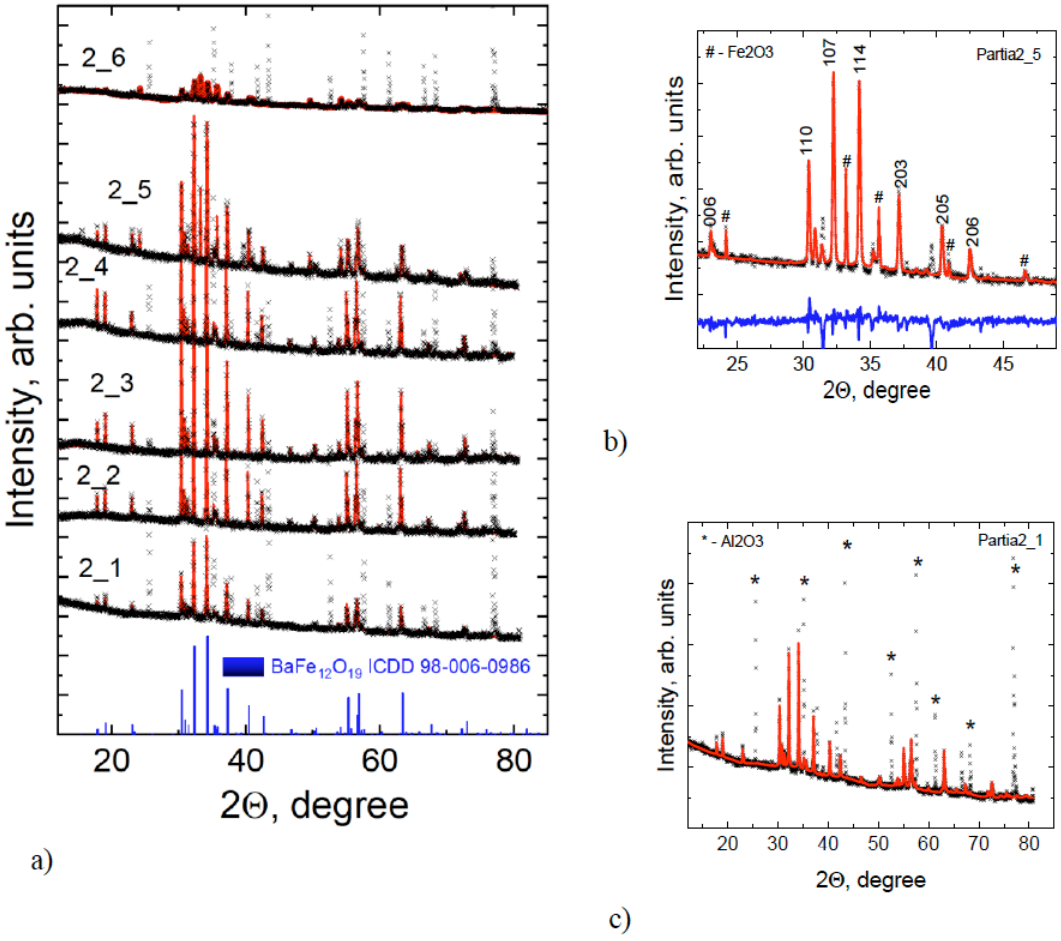


Figure 3: (**a**) general pattern and selected X-ray diffraction patterns of (**b**) 2-5 and (**c**) 2-1 BaM thick film specimens.

incomplete incorporation of iron into the BaM structure. This is consistent with the observed decrease in the lattice parameters of the main phase. Iron depletion causes the unit cell to contract, while excess iron is precipitated as an oxide. Thus, Mode 3 should be considered less favorable from the standpoint of phase formation thermodynamics, whereas Modes 1 and 2 ensure a single-phase structure.

Almost all the X-ray diffraction patterns of the specimens contain the diffraction peaks of the Al_2O_3 substrate (98-007-3725) onto which the films were deposited (Figure **3c**).

The lattice parameters *a* and *c* and the unit cell volume *V* were calculated for all the specimens based on the X-ray diffraction data. Figures **4a** and **4b** show lattice parameter as a function of BaM film thickness.

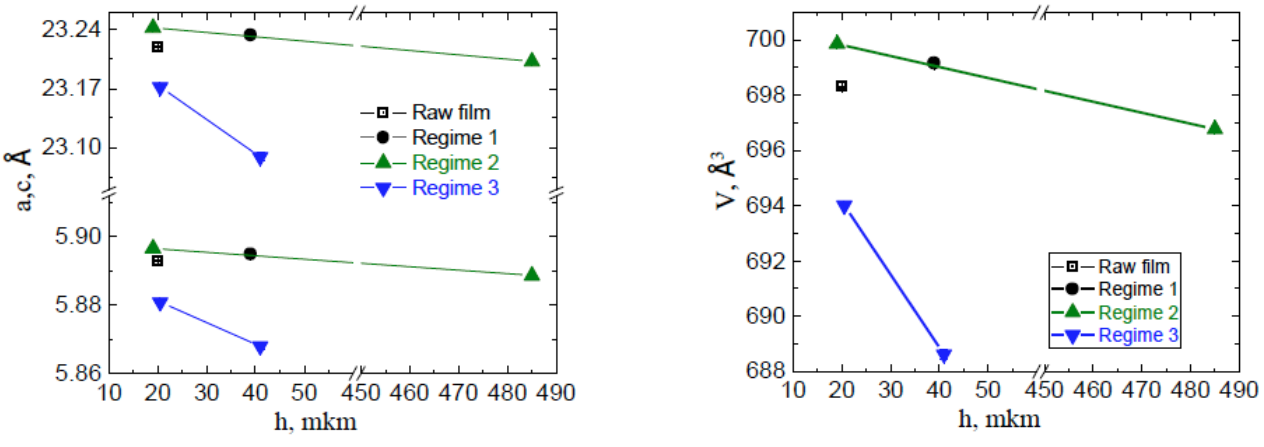
To assess the significance of the observed trends, it is necessary to specify the measurement uncertainties for the crystal lattice parameters, which are ±0.0008–0.001 Å for the a-parameter, ±0.002–0.005 Å – for c, and ±0.01–0.03 $Å^3$ for the unit cell volume. The reported changes in the parameters (in Figure **4**) exceed these uncertainties, which confirms the systematic nature of the dependencies.

The specimens obtained in Modes 2 and 3 exhibit a decrease in the lattice parameter with an increase in the film thickness. For the specimens obtained in Mode 2 an increase in the film thickness from 19 to 485 μm causes a decrease in the lattice parameter *a* from 5.897 Å to 5.889 Å, in the parameter *c,* from 23.242 Å to 23.202 Å, and in the unit cell volume, from 699.85 $Å^3$ to 696.77 $Å^3$ (Figure **4**). A greater decrease in the unit cell volume was observed for the films obtained in Mode 3. An increase in the film thickness from 20.5 to 41 μm causes a decrease in the lattice parameter *a* from 5.881 Å to 5.868 Å, in the parameter *c,* from 23.172 Å to 23.089 Å, and in the unit cell volume, from 694.01 $Å^3$ to 688.64 $Å^3$ (Figure **4**).

The observed decrease in unit cell parameters for modes 2 and 3 can be explained by the relaxation of elastic stresses as the film thickness increases. In the early stages of growth, the thin BaM layer is under stress due to lattice mismatch with the Al_2O_3 substrate (ICDD 98-007-3725) and differences in the thermal expansion coefficients of the contacting materials. As the film thickens, the accumulated elastic energy partially relaxes, which manifests as compression of the unit cell along both directions. A more significant reduction in lattice parameters in Mode 3 ($\Delta V \approx 5.4$ $Å^3$) compared to ≈ 3.1 $Å^3$ in mode 2 indicates either higher initial stress or a different relaxation mechanism—likely associated with the formation of an Fe_2O_3, impurity phase, the presence of which may act as a stress sink and simultaneously indicate a violation of the iron stoichiometry.

The significantly lower values of the crystal lattice parameters for samples 2-5 and 2-6, prepared under Mode 3, compared to Modes 1 and 2 (see Table **1**), may be due not only to stress relaxation but also to a deviation of the chemical composition from stoichiometry; thus, the precipitation of α-Fe_2O_3 indicates an iron depletion in the matrix phase, which leads to a contraction of the $BaFe_{12}O_{19}$ lattice. This effect should be considered in conjunction with the microstructural data (Figure **5**).

Since the specimens were covered with Al_2O_3 wafers during binder evaporation and sintering, oxygen access was restricted. Most probably, the specimens contain oxygen vacancies, and therefore the lattice parameters *a* and *c* are smaller. Limited oxygen access



a) b)

Figure 4: (**a**) Lattice parameters and (**b**) unit cell volume of BaM films obtained in different process modes.

also seems to be the origin of the Fe_2O_3 phase formation in these specimens.

It is noteworthy that, despite the significant difference in the process Modes 1 and 2, the respective X-ray diffraction patterns did not reveal large differences in the crystal structure of the first four specimens obtained in these modes.

The crystallite size and deformation degree of barium hexaferrite films affect the broadening of the diffraction peaks in different manners depending on the interplane spacing d_{hkl}, and hence their contributions can be separated. Figure **5** shows that the experimental points can be well approximated by linear functions the slopes of which depend on film thickness and growth mode, thus indicating the growth of microdeformations in the crystallites. The experimental points shown in Figure **5** correspond to different Miller indexes, thus indicating the absence of anisotropic contribution to the broadening of the diffraction peaks. The microstructural parameters of the barium hexaferrite films were calculated using Eq. (1).

The average crystallite size is between 654 Å and 1136 Å, whereas the microdeformation of almost all the specimens varies from 0.05 % to 0.15 %. The greater figure ε ~ 0.65 % for Specimen 2-6 can originate from its lower quality. Apparently, this value does not reflect the true microdeformation but is an artifact of the approximation: when there are few reflections and they are significantly broadened against the background of the substrate peaks, the separation of the contributions from the dimensional and microdeformation factors becomes unstable.

It can be seen from Figure **3** that the diffraction peaks of barium hexaferrite are far weaker than the substrate reflections, and that the hexaferrite film obtained in Mode 3 is not single-phase and contains the Fe_2O_3 impurity. The specimens obtained in Mode 2 exhibit a decrease in microdeformation from 0.11 to 0.05% with an increase in the average film thickness from 19 to 485 μm, probably due to lower elastic deformation caused by film and substrate lattice parameters mismatch.

It should be emphasized that the lattice parameters were determined at room temperature; therefore, the observed changes reflect residual stresses and structural defects formed as a result of the sample's rapid cooling, rather than as a consequence of thermal expansion. Therefore, to distinguish between the contributions of thermal and intrinsic stresses, future studies will involve temperature-dependent X-ray diffraction measurements and a comparison of the parameters with a reference BaM powder obtained under equilibrium conditions.

The obtained values for crystallite size (654–1136 Å) and microdeformations (0.05–0.15 %) are in good agreement with the stress relaxation profile. For Mode 2, the decrease in ε from 0.11% to 0.05% as the film thickness increases from 19 to 485 μm is accompanied by a small but systematic decrease in the crystal lattice parameters, which is typical for the transition from a stressed thin-film state to a less stressed one. It should be noted that in the Williamson–Hall method, a possible correlation between the contributions of the crystallite size effect and the magnitude of microdeformation in the broadening of diffraction peaks may hinder their separation, for example, in the presence of anisotropy in the broadening. The absence of pronounced anisotropy is confirmed by the fact that the data points in Figure **5a**, for different Miller indices, fit into common linear relationships, confirming that the broadening is essentially isotropic and is associated with the dispersion of crystallites and/or with

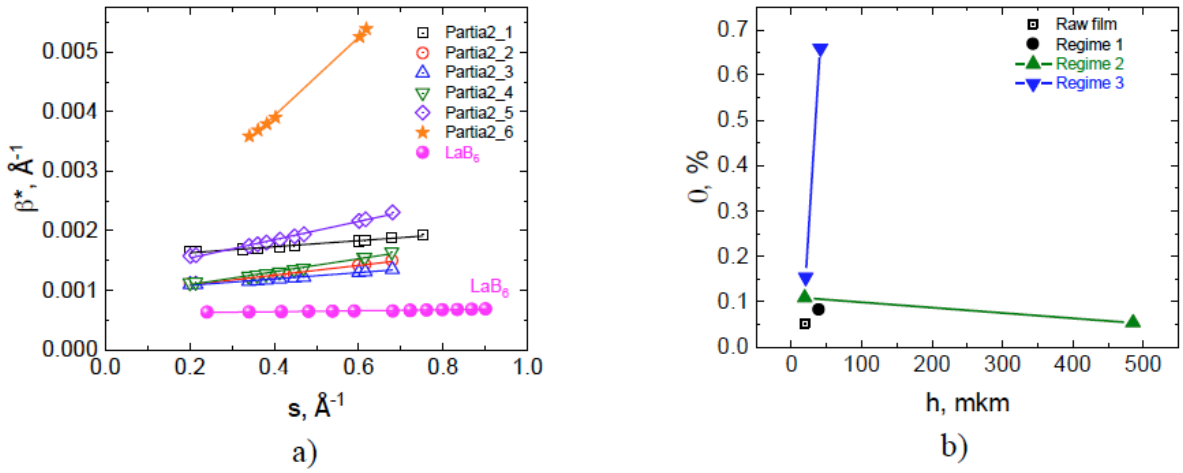


Figure 5: (**a**) Normalized broadening of diffraction peaks $\beta^*(2\theta)= \beta(2\theta)\times\cos(\theta)/\lambda$ as a function of scattering vector $s=2\times\sin(\Theta)/\lambda$ and (**b**) microdeformation of crystallites as a function of barium hexaferrite film thickness for different growth modes.

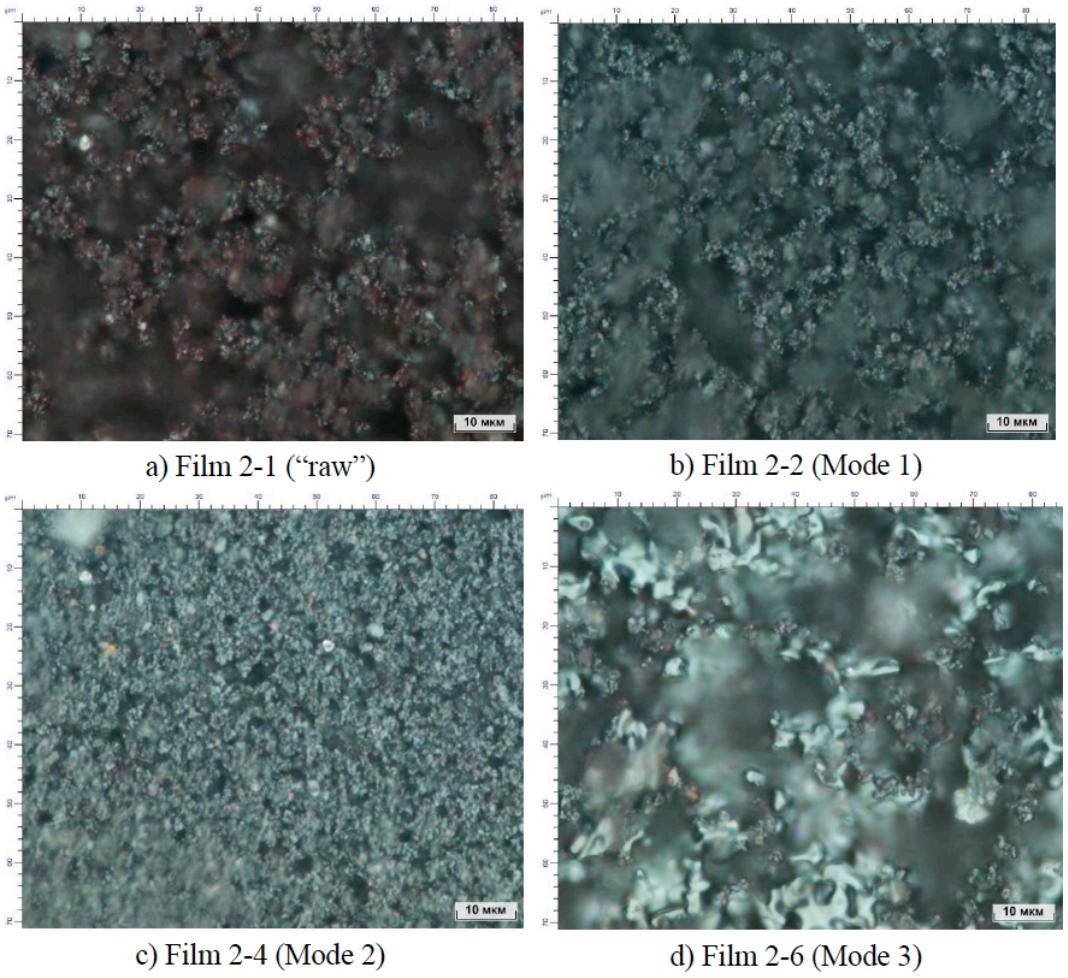


Figure 6: Surface photos of experimental BaM films (1000x magnification).

homogeneous microdeformations, rather than with directional packing defects.

3.2. Surface Quality of Obtained BaM Films

The surface quality of the obtained BaM films was studied under a NexcopeNIM920 optical microscope, China, at a 1000x magnification. Figure **6** shows photos of the BaM film surfaces: a) raw film, b) film 2-2 (Mode 1), c) film 2-4 (Mode 2) and d) film 2-6 (Mode 3).

As can be seen from Figure **6**, the raw specimens furthermore differ in color (red-brown inclusions resolved against the grey background). The other specimens are grey. The specimens (except for 2-4) contain large pores. The pore sizes are especially large in film 2-6 which further confirms the unsuitability of Mode 3. The pores are the smallest in the films obtained in Mode 2.

3.3. Magnetic Properties of Obtained BaM Films

Magnetic hysteresis loops of the test films were recorded at room temperature with a VSM-250 vibrating sample magnetometer from YP Magnetic Technology Development Co., Ltd, China.

The magnetic texture degree *f* of the test specimens was calculated based on the hysteresis loop parameters using Eq. (2) [23].

Figure **7** shows the magnetic hysteresis loops of film 2-1 (raw film), film 2-2 (growth Mode 1) and films 2-3 and 2-4 (growth Mode 2).

Figure **8** shows the magnetic hysteresis loops of film 2-1 (raw film), film 2-2 (growth Mode 1), film 2-4 (growth Mode 2) and films 2-5 and 2-6 (growth Mode 3). Table **2** summarizes the main magnetic parameters of all the six films.

As can be seen from Figures **7** and **8** and Table **2**, the highest figures of the most important magnetic parameters (specific saturation magnetization σ_s and coercive force ${}_iH_c$) are observed for specimens 2-2, 2-3 and 2-4 grown in process Modes 1 and 2. The σ_s figure of these specimens is within 73-76 emu/g for magnetization in the film plane and 70-74.5 emu/g for magnetization perpendicular to the film plane; ${}_iH_c$ is within 3.03-3.08 kOe for magnetization in the film plane and 2.74-3.06 kOe for magnetization perpendicular to the film plane. These σ_s and ${}_iH_c$ figures are typical of high-quality hexagonal $BaFe_{12}O_{19}$ ferrites [2, 5]. The

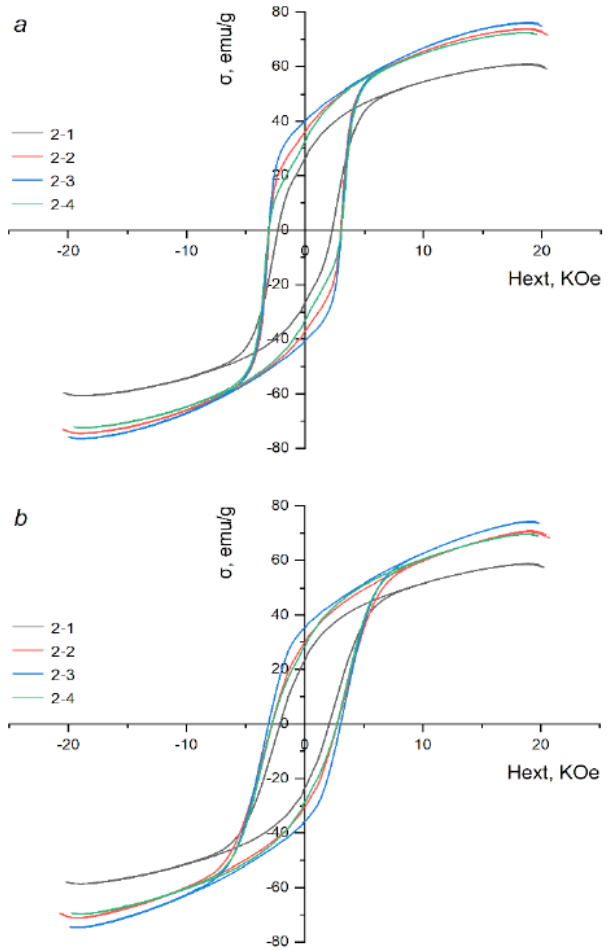


Figure 7: Magnetic hysteresis loops of BaM films obtained in different process modes: 2-1 is “raw” film; 2-2 is film grown in Mode 1; 2-3 and 2-4 are films grown in Mode 2. **a**) field H∥ of film plane; **b**) field H⊥ of film plane.

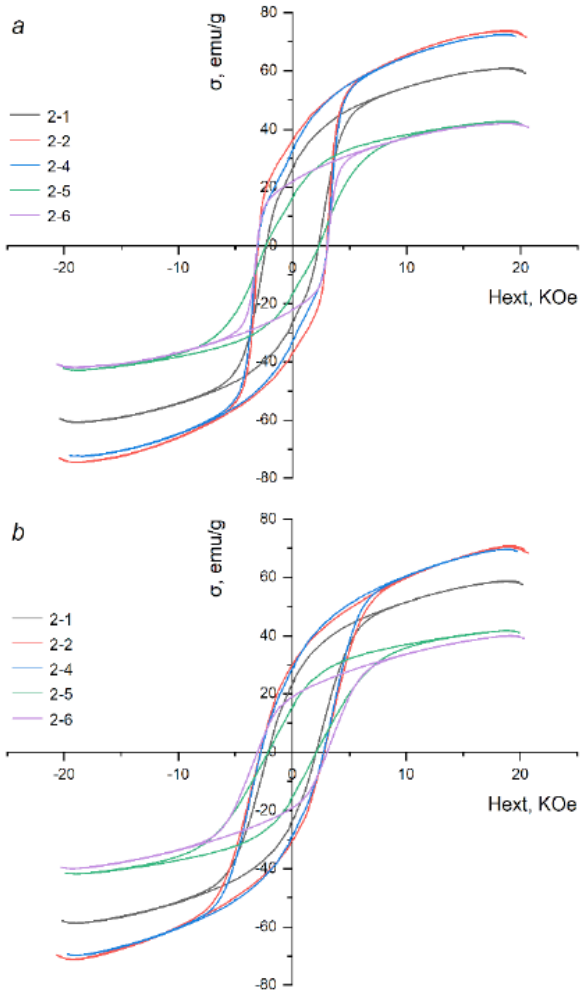


Figure 8: Magnetic hysteresis loops of BaM films obtained in different process modes: 2-1 is “raw” film; 2-2 is film grown in Mode 1; 2-4 is film grown in Mode 2; 2-5 and 2-6 are films grown in Mode 3. **a**) field H∥ of film plane; **b**) field H⊥ of film plane.

specific saturation magnetization of the “raw” film is 18% lower than the average σ_s of films 2-2, 2-3 and 2-4. The lowest specific saturation magnetization and specific remanence magnetization are observed for films 2-5 and 2-6 (Table **2** and Figure **8**). The average σ_s of these films is 43% lower than the average figure for specimens 2-2, 2-3 and 2-4, and 30% lower than that of the raw film specimen (2-1). These specific features of films 2-5 and 2-6 can be accounted for by the presence of a second phase (Fe_2O_3) in these specimens. The magnetic moment of the unit cell of α-Fe_2O_3 is tens of times smaller than the magnetic moment of the unit cell of $BaFe_{12}O_{19}$. In this regard, the presence of α-Fe_2O_3 oxide in barium hexaferrite, even at the level of measurement accuracy (5% weight for XRD), will significantly affect the value of the specific saturation magnetization and, naturally, the intensity of the magnetic hysteresis loop, which is what we observe.

It can also be seen from Table **2** that the magnetic texture degree of the experimental films is within 8.0 – 15.76 %. Thus, the specimens are isotropic. This is also confirmed by the absence of <008> reflections in their X-ray diffraction patterns [24], which precludes more accurate determination of the magnetic texture degree from the X-ray diffraction patterns. The moderate magnetic texture degree of isotropic barium hexaferrites [25] is accounted for by the flake-like shapes of the hexaferrite particles forming during ferritization. During pressing of raw isotropic hexaferrite billets, these particles are oriented perpendicular to the pressing direction axis, despite the absence of magnetic field. As a result, a texture forms, the degree of which increases slightly during sintering.

4. CONCLUSIONS

In this work, isotropic polycrystalline barium hexaferrite $BaFe_{12}O_{19}$ films with thicknesses of 19, 20, 39, 41 and 485 μm were grown in three process modes on Al_2O_3 substrates. The crystal structure, surface quality and magnetic hysteresis loop parameters of the specimens were studied. The best parameters were

Table 2: Magnetic Parameters of Experimental BaM Films

Specimen	PARAMETERS										Notes
	h, μm	H_k, Oe		σ_s, emu/g		σ_r, emu/g		$_iH_c$, kOe		f, %	
		$H_{\parallel}$	$H_{\perp}$	$H_{\parallel}$	$H_{\perp}$	$H_{\parallel}$	$H_{\perp}$	$H_{\parallel}$	$H_{\perp}$		
2-1	20	3040	3265	61	59	26	23	2.30	2.09	8.35	"Raw"
2-2	39	3375	4050	74	71	36	30	3.03	2.78	10.85	Mode 1
2-3	485	3655	4595	76	74.5	40	35	3.08	3.06	15.76	Mode 2
2-4	19	3375	4030	73	70	33	28	3.07	2.74	11.82	Mode 2
2-5	20.5	3975	3890	43	42	16	15	2.35	2.10	9.10	Mode 3
2-6	41	3580	4615	42	40	22	19	3.10	3.05	8.00	Mode 3

Table notations: h is film thickness; H_k is effective magnetic anisotropy field; σ_s is specific saturation magnetization; σ_r is specific remanence magnetization; $_iH_c$ is magnetization coercive force; f is magnetic texture degree.

observed for the specimens grown in process Mode 2. The films grown using this technology have parameters typical of high-quality bulk polycrystalline $BaFe_{12}O_{19}$. The quality of the experimental specimens is far higher than that of the specimens obtained by the Authors earlier [26].

Obtaining high-quality BaM hexaferrite films with large area and thicknesses ranging from ~20 μm to over 480 μm is a very important result for microwave electronics. Such films can be effectively used in the production of circulators, phase shifters, resonators, and filters. Of particular value is the fact that film hexaferrites can be widely integrated into planar technologies for producing semiconductor devices in the manufacture of instruments containing ferrite and semiconductor elements.

In terahertz spectroscopy and terahertz photonics, thick BaM films will find application as non-reciprocal Faraday isolators designed to protect sources of electromagnetic radiation from the effects of back-reflected light.

ADDITIONAL INFORMATION

The Authors declare that no AI tools were used in the preparation of the manuscript.

FUNDING

The work was carried out at the expense of funds provided under Grant No. 24-13-00268 of the Russian Scientific Foundation.

AUTHOR´S CONTRIBUTION STATEMENT

The Authors declare that there is no conflict of interests.

REFERENCES

[1] Letyuk L.M., Kostishin V.G., Gonchar A.V. Technology of Ferrite Materials of Magnetoelectronics. Moscow: MISIS; 2005. 352 p. [in Russian].

[2] Smit J., Wijn H. Ferrites. Physical Properties of Ferrimagnetic Oxides in Relation to Their Technical Applications. Eindhoven: Philips Technical Library; 1959. 369 p.

[3] Altman A.B., Vernikovsky E.E., Gerber A.N., Gladyshev P.A., *et al*. Permanent Magnets. Handbook. Moscow: Energiya; 1980. 488 p. [in Russian].

[4] Mishin D.D. Magnetic Materials: Textbook for Universities. Moscow: Vysshayashkola; 1991. 384 p. [in Russian].

[5] Pullar R.C. Hexagonal ferrites: a review of the synthesis, properties, and applications of hexaferrite ceramics. Progress in Materials Science. 2012; 57(7): 1191-1334. https://doi.org/10.1016/j.pmatsci.2012.04.001

[6] Pardavi-Horvath M. Microwave applications of soft ferrites. Journal of Magnetism and Magnetic Materials. 2000; 215-216: 171-183. https://doi.org/10.1016/S0304-8853(00)00106-2

[7] Harris V.G. Modern microwave ferrites. IEEE Transactions on Magnetics. 2012; 48(3): 1075-1104. https://doi.org/10.1109/TMAG.2011.2180732

[8] Ustinov A., Kochemasov V., Khasyanova E. Ferrite materials for microwave electronic devices. Main selection criteria. Electronics NTB. 2015; (8): 86-92. [in Russian]

[9] Shalaby M., Peccianti M., Ozturk Ya., Morandotti R. A magnetic non-reciprocal isolator for broadband terahertz operation. Nature Communications. 2013; 4: 1558. https://doi.org/10.1038/ncomms2572

[10] Petrov V.V., Ivanova V.I. Hexaferrites - a promising material for microwave devices in the millimeter wavelength range. In: Proceedings of the XXIII All-Russian Conference "Electromagnetic Field and Materials (Fundamental Physical Research)". Moscow: INFRA-M; 2015. p. 7-24. [in Russian].

[11] Medvedev S.A., Pollak B.P., Cheparin V.O., *et al*. Development, research, and application of hexaferrite single crystals—new microwave radio materials. In: Reports of the Scientific and Technical Conference on the Results of Research in 1968-69. Radio Engineering Section. Moscow: MPEI; 1969. [in Russian].

[12] Harris V., Chen Z., Chen Y., *et al*. Ba-hexaferrite films for next generation microwave devices (invited). Journal of Applied Physics. 2006; 99(8). https://doi.org/10.1063/1.2165145

[13] Capraro S., Chatelon J., Le Berre M., *et al*. Barium ferrite thick films for microwave applications. Journal of Magnetism and Magnetic Materials. 2004; 272-276(Suppl. 1). https://doi.org/10.1016/j.jmmm.2003.12.871

[14] Zhang X., Yue Z., Li L., Am J. Orientational growth and magnetic properties of BaM hexaferrite films deposited by direct current magnetron sputtering. Journal of the American Ceramic Society. 2016; 99: 860-865. https://doi.org/10.1111/jace.14007

[15] Chen D., Wang G., Chen Z., *et al*. Highly c-axis oriented, self-biased and low loss barium ferrite thin films by sol-gel method. Materials Letters. 2017; 189: 229-231. https://doi.org/10.1016/j.matlet.2016.12.026

[16] Yu C., Sokolov A., Kulik P., *et al*. Stoichiometry, phase, and texture evolution in PLD-grown hexagonal barium ferrite films as a function of laser process parameters. Journal of Alloys and Compounds. 2020; 814: 152301. https://doi.org/10.1016/j.jallcom.2019.152301

[17] Fan L., Zheng H., Shen S., *et al*. Film-thickness dependence of the morphology, crystal structure and magnetic properties of $BaFe_{12}O_{19}$ films prepared by pulsed laser deposition. Journal of Electronic Materials. 2019; 48: 5717-5722. https://doi.org/10.1007/s11664-019-07378-1

[18] Chen T., Chen Y., Sakai T., *et al*. Screen printed thick self-biased, low-loss, barium hexaferrite films by hot-press sintering. Journal of Applied Physics. 2006; 100(4): 043907. https://doi.org/10.1063/1.2221527

[19] Levin B.E., Tretyakov Yu.D., Letyuk L.M. Physicochemical Principles of Obtaining, Properties and Application of Ferrites. Moscow: Metallurgiya; 1979. 473 p. [in Russian].

[20] Degen T., Sadki M., Bron E., König U., Nénert G. The HighScore suite. Powder Diffraction. 2014; 29(S2): S13-S18. https://doi.org/10.1017/S0885715614000840

[21] Rodríguez-Carvajal J., Roisnel T. Line broadening analysis using Full Prof*: determination of microstructural properties. Materials Science Forum. 2004; 443-444: 123-126. https://doi.org/10.4028/www.scientific.net/MSF.443-444.123

[22] International Centre for Diffraction Data (ICDD). PDF-2 Release 2024. Newtown Square, PA, USA: ICDD; 2024. Available from: http: //www.icdd.com/[cited 2026 Sep 20].

[23] Timofeev A.V., Kostishin V.G., Chitanov D.N. Influence of the technology for producing ferritized powder on the degree of magnetic texture of $BaFe_{12}O_{19}$ and $SrFe_{12}O_{19}$ hexaferrite plates. Pisma v ZhTF. 2019; 45(8): 34-36. [in Russian]. https://doi.org/10.1134/S106378501904031X

[24] Kostishyn V.G., Trukhanov A.V., Alekseev A.A., Scherbakov S.V., *et al*. Crystal and magnetic structure of hexagonal anisotropic polycrystalline ferrites $SrFe_{12}O_{19}$ obtained by radiation-thermal sintering. Modern Electronic Materials. 2025; 11(2): 111-123. https://doi.org/10.3897/j.moem.11.2.163141

[25] Kaneva I.I., Kostishin V.G., Andreev V.G., Chitanov D.N., *et al*. Obtaining barium hexaferrite brand 7BI215 with isotropic properties. Izvestiya Vysshikh Uchebnykh Zavedenii. Materialy Elektronnoi Tekhniki = Materials of Electronics Engineering. 2015; (3): 183. [in Russian]. https://doi.org/10.17073/1609-3577-2014-3-183-188

[26] Kostishin V.G., Sysoev M.A., Isaev I.M., Prusakov A.D. Investigation of the structure and magnetic properties of thick $BaFe_{12}O_{19}$ films obtained by slip casting. Zavodskaya Laboratoriya. Diagnostika Materialov. 2026; 92(4): 50-54. [in Russian]. https://doi.org/10.26896/1028-6861-2026-92-4-50-54

https://doi.org/10.31875/2410-4701.2026.13.10

© 2026 Kostishin *et al.*
This is an open-access article licensed under the terms of the Creative Commons Attribution License (http://creativecommons.org/licenses/by/4.0/), which permits unrestricted use, distribution, and reproduction in any medium, provided the work is properly cited.